Development of an aerodynamic analysis tool for boundary layer ingestion concept design

33RD CONGRESS
OF THE INTERNATIONAL COUNCIL
OF THE AERONAUTICAL SCIENCES
STOCKHOLM, SWEDEN, 4–9 SEPTEMBER, 2022

ICAS 2022 SWEDEN

Development of an aerodynamic analysis tool for boundary layer ingestion concept design

Xin Zhao[1], Carlos Xisto[1], Shia-Hui Peng[1,2]

[1]Chalmers University of Technology, Sweden
[2] Swedish Defence Research Agency (FOI)

Abstract

The methods incorporated in an aerodynamic analysis tool are introduced to support aircraft conceptual designs, where a boundary layer ingestion (BLI) propulsion system is deployed. In order to integrate the BLI model to a generic tool for aircraft designs, two methods of approximating boundary layer profiles along the airframe/fuselage have been examined. For an airfoil-shaped wing/body configuration, the airfoil analysis program XFOIL is used and, alternatively, the flat plate boundary layer theory may be adopted. With the boundary layer characteristics approximated from these methods, the fan performance in terms of pressure ratio and efficiency is corrected considering the inflow distortion incurred by the boundary layer ingested, based on a simplified parallel compressor method. Given the corrected fan pressure ratio and efficiency, an equivalent velocity bookkeeping method is used for predicting the BLI fan performance in terms of power requirement and thrust generation. A validation against the boundary layer approximation is also presented in comparison with the RANS-based CFD simulations for a blended wing body (BWB) aircraft.

Keywords: Boundary layer ingestion (BLI), Conceptual aircraft design, Aerodynamic analysis

1. Introduction

To assess the potential and ultimately to establish a roadmap towards the maturation of electric propulsion (EP) and hybrid electric propulsion (HEP) architectures, the integration of relevant up-to-date methodologies and technologies is a critical step. Among others, boundary layer ingestion (BLI) propulsion is an emerging technology that has attracted attention for its potential in fuel savings – particularly in conjunction with EP/HEP aircraft. In recent years, BLI propulsors have been widely considered and explored in revolutionary designs of next-generation aircraft, such as in designs of blended wing body (BWB) and distributed electric propulsion (DEP) configurations [1-4]. For aircraft propulsion concepts facilitating different degrees of electrification, previous studies have shown that BLI may play as an important benefit booster [5-7].

By means of a compact aero-propulsive integration, BLI propulsors are usually attached on the airframe and allow low momentum boundary layer flows ingested and energized. The use of BLI technology triggers changes in the aircraft aerodynamic and propulsive performance [8]. These include, among others, increased propulsive efficiency of the engine, reduced nacelle and pylon drag, as well as mitigated wake mixing. Moreover, the adoption of BLI modifies the aerodynamic features over the near-ingestion airframe surface (and thus associated skin-friction drag and surface pressure) and, furthermore, may lead to a reduced total pressure recovery and increasing distortion at the inlet exit. These aspects are often used as indications in assessing the BLI design. Unlike conventional non-BLI propulsion systems, a BLI configuration requires particular attention to the airframe-engine integration already in the stage of conceptual design.

1.1 Scope of the work

The BLI analysis tool presented in this paper has been developed on the basis of the previous studies of BLI [8-17]. The main purpose is to support the conceptual design at low technology readiness levels (TLR = 1-2) of unconventional aircraft configurations with BLI propulsors. The drag and thrust force balance method has been taken as the basis of the model incorporated [13, 18]. With

predefined thrust requirement and aircraft aerodynamic performance, the BLI effect is assessed through its influence on the generation of propulsive force. In the following sections, the major aspects deployed in building and exploring the model are introduced, including generic 3D geometry simplification and discretization of the baseline aircraft model, estimation of discretized airframe aerodynamic performance through 2D approximation, approximation of boundary layer characteristics, and prediction of BLI fan performance using an equivalent velocity bookkeeping method. The BWB geometry created by Brown [19] has been reproduced as a baseline model for verifying the BLI model developed in this work for a demonstration. The same BWB configuration has also been adopted in a set of CFD simulations, which serve in this work a preliminary validation of the boundary layer characteristics approximated from the BLI model at a selected angle of attack (AoA).

1.2 Baseline aircraft model

The baseline BWB aircraft model (with no BLI) targets a short-range, 150 PAX design for a cruise Mach number of 0.75 [19]. Figure 1 shows a schematic drawing of the baseline BWB model with some of the main dimensions, while Table 1 lists the overall dimensions and geometrical parameters.

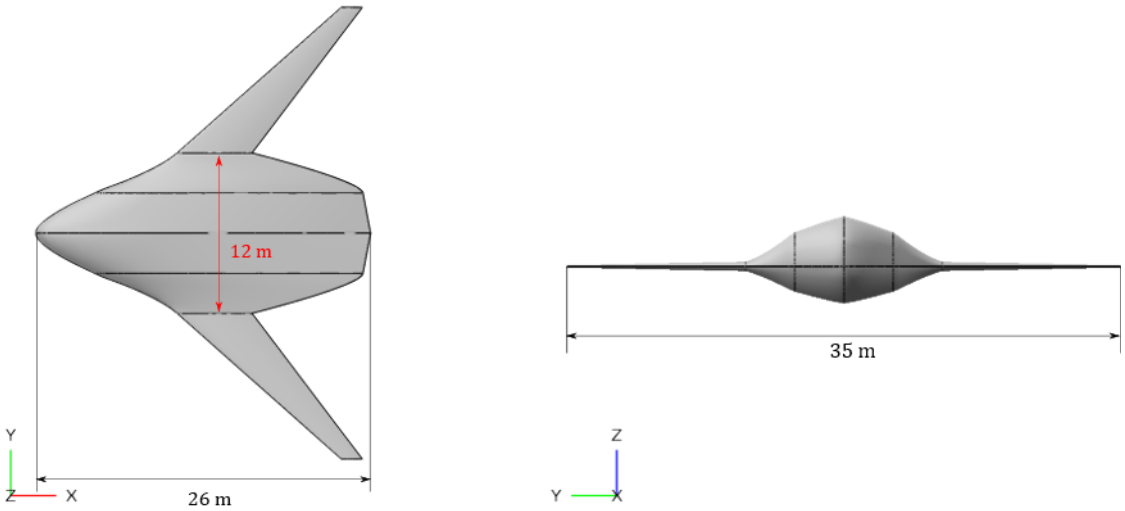

Figure 1 – Top-view (Left) and front-view (Right) of the 150PAX BWB aircraft model used for validation in this work.

Table 1: Overall dimensions and geometrical parameters of the BWB.

Sref	311	m^2
Span	35	m
Length	26	m
MAC	17.2	m
Λ_le_out	48.5	deg
W/L	200	kg/m^2
Centerbody airfoil	NACA 23021	[-]
Wing airfoil	NASA SC(2)-0410	[-]

2. Methods and Approximations

In this section, the details of the methods used in the BLI analysis tool are given. Since the model is intended to be applicable for generic aircraft geometries including BWB and tube-and-wing-body (TWB) configurations, the approximation in discretizing the aircraft geometry into key cross-sections for boundary layer development is described. After defining the engine installation position, different

methods are then presented for estimating boundary layer characteristics at the corresponding position of all the cross-sections. With the information, analysis can be conducted on the BLI fan performance using the equivalent velocity bookkeeping method, and the velocity/total pressure profiles of the boundary layer approximated are also illustrated in comparison with CFD simulations.

2.1 Generic 3D geometry simplification and discretization

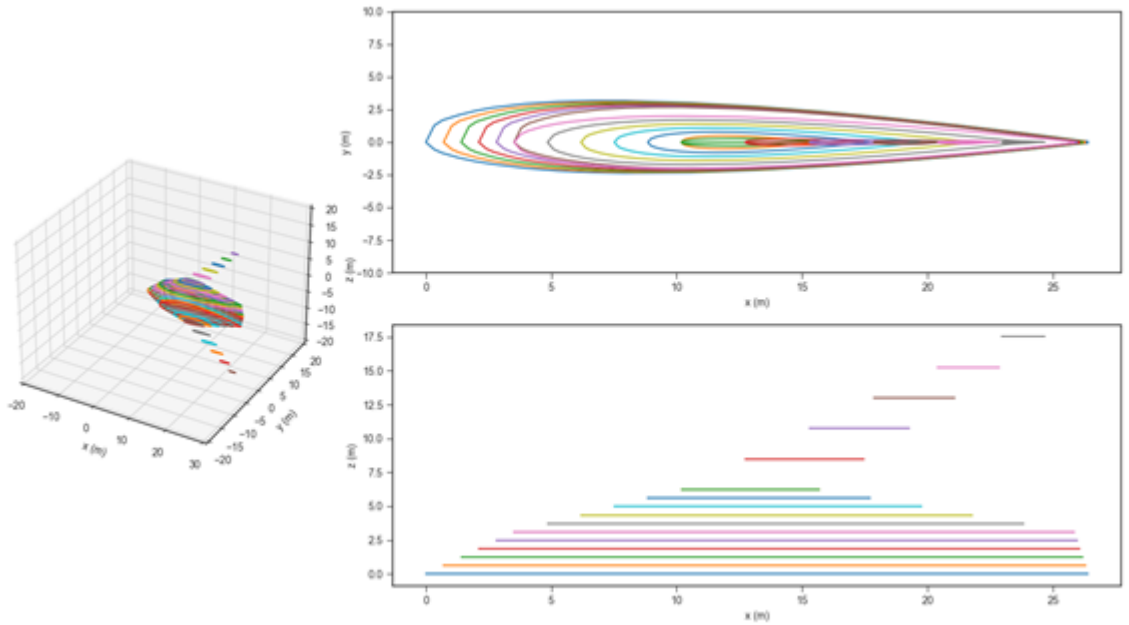

Figure 2 Example of BWB simplification and discretization

The general idea of the 2D simplification of a 3D geometry, such as a BWB body, is to split the aircraft into a set of spanwise zones, i.e. fuselage, transition (wing-body junction) and wing, then discretizing each zone with basic 2D elements. With the baseline BWB described above, for example, the cross-section of each zone can be treated as a specific type of 2D airfoil. Through defining the number of cross-sections for each zone, several 2D airfoils with different chords could represent the general outline of the geometry, as shown in Figure 2. These basic 2D airfoils are then analyzed by the airfoil design and analysis program XFOIL [20]. For other non-airfoil shaped zones, like the fuselage part of a TWB, the estimation of its boundary layer characteristics refers to the boundary layer over a flat plate with necessary corrections upon the geometric and flight conditions. No additional discretization is needed and only the streamwise length will be transferred in the estimation of boundary layer characteristics.

2.2 Estimation of airframe boundary layer characteristics

Obtaining the boundary layer characteristics in terms of velocity profile and total pressure profile of the fan inlet flow is critical in order to evaluate the BLI effects using the thrust accounting method. The left figure in Figure 3 shows a 2D representation of the boundary layer velocity profile entering a fan. After the discretization of the airframe, the 2D boundary layer velocity profile could be obtained for the position where the engine is installed at each of the cross-sections. For attached boundary layer flows, a 3D representation of the inlet velocity profile, as illustrated in the right-hand-side figure of Figure 3, is formed by integrating the calculated 2D profiles. Two methods for the calculation of key characteristics of a 2D boundary layer are described below. Based on the output from the two methods, a crude approximation of the boundary layer velocity profile is introduced, which can be used to estimate the BLI mass flow rate for conceptual design.

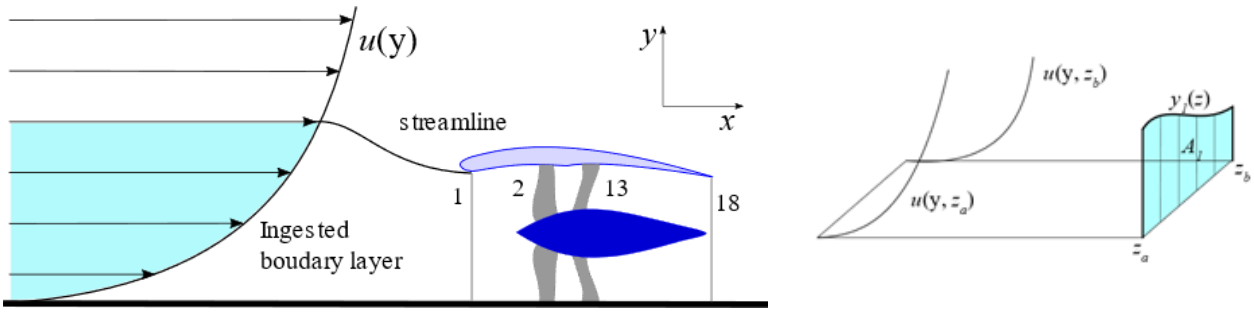

Figure 3 Example of ingested boundary layer, 2D representation (left), 3D representation (right). Station numbering in the left figure used for calculating engine performance.

2.2.1 Airfoil analysis tool

The first method utilizes the airfoil design and analysis tool – XFOIL [20] to obtain boundary layer related characteristics, such as displacement thickness, momentum thickness and shape factor, which are used to approximate the boundary layer velocity profile. Even though the tool was originally created for the rapid analysis of low Reynolds number airfoil flows with transitional separation bubbles, comparisons between the model results and the CFD results at high Reynolds number applications have shown good agreement. With the input airfoil coordinate file, the geometry of the airfoil shape is divided into individual panels within XFOIL. After defining other necessary inputs - Mach number, Reynolds number and AoA, a viscous solution can be formulated. As the true boundary layer and local velocity profiles are not built-in outputs, post-processing of the XFOIL output is required.

General approximation of boundary layer thickness, typically, using displacement thickness and/or momentum thickness can be found in many textbooks and other literature. Two of these approximations have been considered to conclude the optimal approximation in comparison with the CFD results. One is based on a recent contribution from Budziszewski and Friedrichs [10] who also utilize XFOIL in their BLI propulsor modelling. For their approximation, the boundary layer thickness, δ_{BL} can be calculated from the boundary layer momentum thickness, θ, and displacement thickness, δ^*, as given below.

$$\delta_{BL} = \frac{\delta^{*2}}{(\delta^* - \theta)} \qquad (1)$$

This approximation, however, in general gives less than half of the boundary layer thickness as predicted by CFD. Alternatively, as given below, Groves [21] in his study proposed an integral prediction method for three-dimensional turbulent boundary layers on rotating blades.

$$\delta_{BL} = \delta^* \left(\frac{2H}{H-1} + H\right) = \frac{\delta^{*2}(H+1)}{(\delta^* - \theta)} \qquad (2)$$

where *H* is the shape factor which is equal to the ratio between the displacement thickness δ^* and momentum thickness θ. Comparing Equation (2) against Equation (1), a difference of factor H+1 is clearly observed. This one serves as the best practice of approximating boundary layer thickness in comparison with CFD results.

The convergence of the BLI analysis tool may become difficult for a case combining high AoAs, high Reynolds number and Mach number. For the test cases performed, at a high Reynolds number (~ 200 million) and high Mach (0.75), however, the convergence at typical AoAs (≤ 5 deg) in level flight is good. At very high AoAs and Mach numbers, additional attention should be paid for convergence in relation to boundary layer separation and/or in the presence of transonic shock waves.

2.2.2 Boundary layer over fuselage surface

For streamlined shape of fuselage, the estimation of boundary layer thickness may be referred to the boundary layer over a flat plate, where the BL thickness is often taken as a function of the local Reynolds number based on the incoming flow velocity and the distance to the leading edge. This is then further corrected with a form factor to account for flow acceleration and possible diffusion due to geometric shape effects. To avoid further complications and as it is in most applications with high Re numbers, we assume the boundary layer is fully turbulent so that the equation below can be used:

$$\delta_{BL} = 0.37 \times Re^{-1/5} \qquad (3)$$

where x is the distance from the fuselage leading edge to the engine installation position. The form factor adopted here is for slender body given in terms of the length to diameter ratio for the body [22].

$$Form\ Factor = 1 + \frac{1.5}{(Length/Diameter)^{2.2}} + \frac{7}{(Length/Diameter)^{3.8}}$$

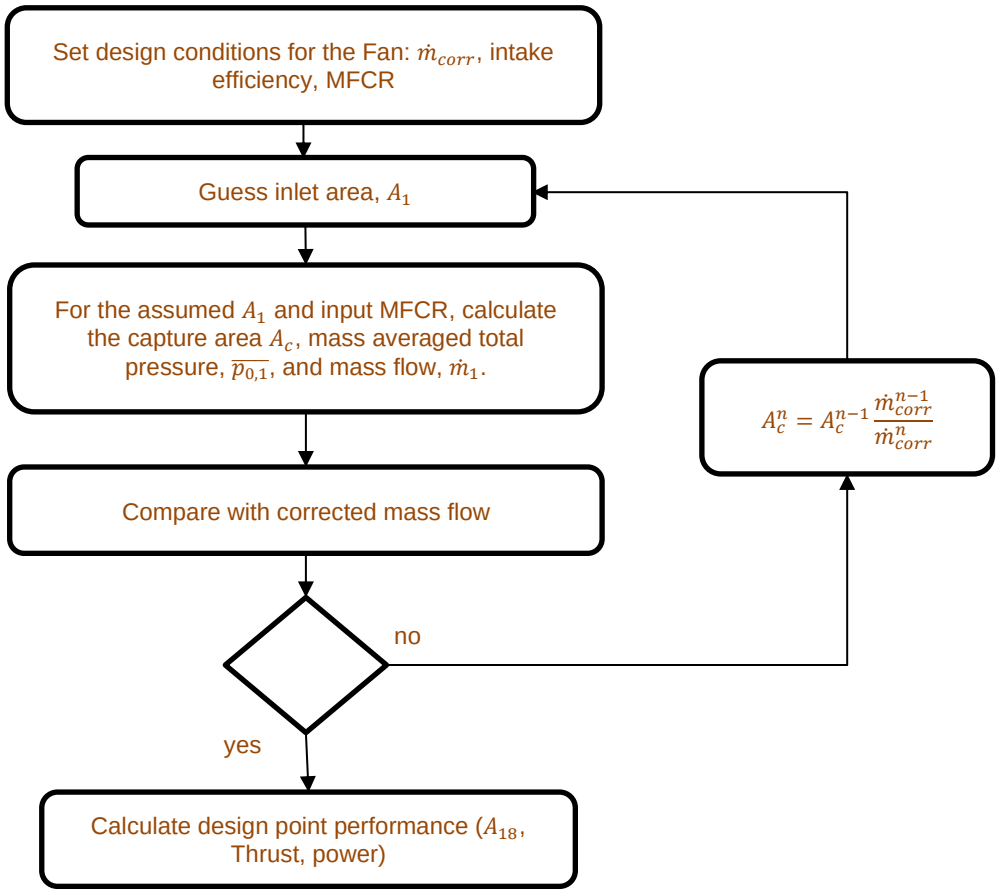

Figure 4: Procedure to calculate engine performance in design, including the procedure for calculating the capture area.

2.2.3 Boundary-layer velocity profiles

With the boundary layer thickness given in Equation (3), the velocity profile is approximated using the 1/7th power law.

$$\frac{u}{U} = \left(\frac{y}{\delta_{BL}}\right)^{1/7} \qquad (4)$$

where u represents the streamwise velocity at corresponding cross-stream spatial coordinate and U

is the freestream velocity. By assuming a constant static pressure across the boundary layer, the profile of the total pressure can be readily established from the velocity profile.

With the boundary layer profiles generated, the iteration loop given in Figure 4is then used in the design to find the captured area. The fan performance is set by the corrected mass flow $\dot{m}_{corr}$. The iteration loop requires mass flow capture ratio (MFCR), and intake efficiency as inputs to calculate the capture area together with the guessed inlet area A_1 to meet the specified corrected mass flow $\dot{m}_{corr}$.

2.3 Analysis of BLI Fan Performance

Supported with the velocity and total pressure profiles of the fan inlet flow, the BLI fan performance can be predicted using the equivalent velocity bookkeeping method. The spanwise variation is insignificant when performing the profiles integration, as shown in the comparison of both the CFD result and the BLI model analysis in Section 3 for the positions at 70% and 80% of the fuselage length. Spanwise variation in the boundary layer becomes significant at the position close to the end of the fuselage, however. This is caused by the trailing edge effect, which is undesirable in designs to locate the engine intake. Some corrections should be further incorporated in future work.

Through integrating the total pressure profile, the mass averaged total pressure entering the fan $\overline{p_{0,1}}$ (station 1 in Figure 3) is obtained, while the total temperature $\overline{T_{0,1}}$ at the fan inlet can be calculated by giving a recovery factor. Within the tool, the recovery factor can either be given as an input or be approximated with the Prandtl number. With the inlet total pressure and total temperature, the mass averaged equivalent velocity $\overline{V_{eq}}$,defined blow, can be estimated.

$$\overline{V_{eq}} = \overline{M_{eq}}\sqrt{\gamma R \overline{T_{eq}}} \tag{5}$$

$$\overline{T_{eq}} = \frac{\overline{T_{0,1}}}{\left(\frac{\overline{p_{0,1}}}{p_\infty}\right)^{\frac{\gamma-1}{\gamma}}}, \tag{6}$$

$$\overline{\mathrm{M}_{eq}} = \sqrt{\frac{2}{\gamma-1}\left[\left(\frac{\overline{p_{0,1}}}{p_\infty}\right)^{\frac{\gamma-1}{\gamma}} - 1\right]}, \tag{7}$$

where p_∞ is the freestream static pressure, $\overline{T_{eq}}$ is the mass averaged equivalent static pressure and $\overline{\mathrm{M}_{eq}}$ is the mass averaged equivalent Mach number. With the mass averaged equivalent velocity, the net thrust generated by the BLI propulsor can be calculated by:

$$F_{net} = F_{gross} - \dot{m}_1 \overline{V_{eq}}, \tag{8}$$

The gross thrust generated by the nozzle (station 18 in Figure 3) is given by:

$$F_{gross} = \int_{A_{18}} (p_{18} - p_{amb}) + \rho V_{18}^2 \, dA, \tag{9}$$

where A_{18} is the nozzle area, p_{18} is the static pressure at the nozzle arising from incomplete expansion to p_{amb} (choked nozzle) and V_{18} is the nozzle jet velocity. As the gross thrust is solely determined by engine performance, a key factor to be considered here is the fan performance

correction due to the inlet flow distortion. Here in this model, a simplified parallel compressor model is used for the mean operating point of the fan. Different from using the flow sector angles [10], the flow areas (free flow area and distorted flow area) are used as shown in Equation (10).

$$\bar{\phi} = \phi_{\text{dist}} \cdot \frac{A_{\text{dist}}}{A_{\text{Inlet}}} + \phi_{\text{freeflow}} \cdot \frac{A_{\text{freeflow}}}{A_{\text{Inlet}}} \,, \qquad (10)$$

where ϕ represents the pressure ratio or efficiency of the fan, and A is the area. With a bar over the symbol gives the mean value of the parameter, while the subscripts "dist", "freeflow" and "Inlet" indicate distorted part, free flow part and the entire inlet, respectively. Instead of matching the operating point throughout the entire fan performance map, one of the running lines is used for the fan performance correction calculation. Typically, the running line with *N* = 100% can be selected.

3. CFD simulations

With the baseline BWB configuration, a set of CFD computations have been performed. The primary purpose with these computations has been to support the analysis of the tool in validating and verifying the aerodynamic components of the BLI analysis methods. Moving beyond, it is anticipated that an extended BLI modelling should be required in conceptual design in order to account for possible alternations in the aerodynamic flow around the aircraft body at relatively large AoAs and/or in the presence of, for example, side slip and gusts. Further analysis will thus be made to explore how the BLI modelling can be extended and improved with the support of reliable CFD data.

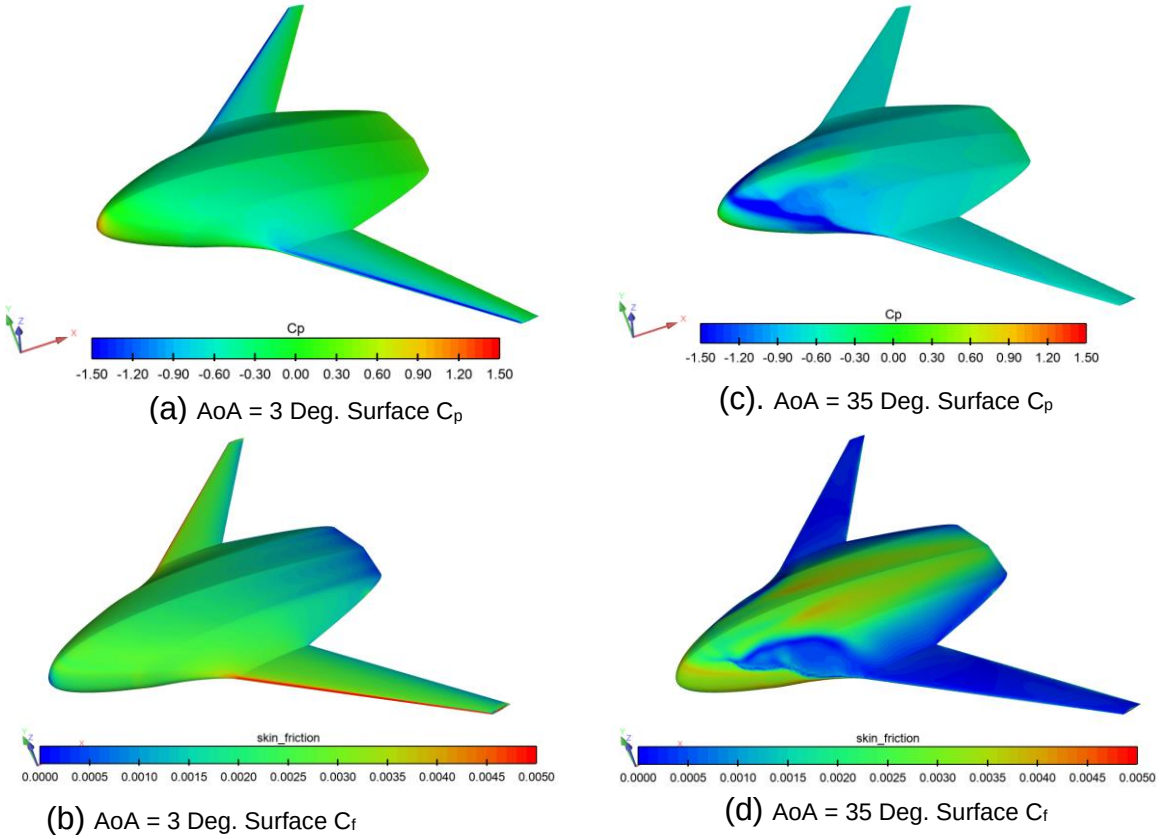

(a) AoA = 3 Deg. Surface C_p

(c). AoA = 35 Deg. Surface C_p

(b) AoA = 3 Deg. Surface C_f

(d) AoA = 35 Deg. Surface C_f

Figure 5: Examples of CFD simulations. Surface pressure and skin friction coefficients at AoA = 3 and AOA = 35 deg.

The CFD computation has been performed for a set of AoAs in a range from 0 to 40 deg at M_∞ = 0.75 and Alt = 10000 m. The computation invokes a half model of the BWB configuration, using a mesh with about 1.65 million nodes. Steady RANS computations are conducted using a k-ω based EARSM

to deal with the turbulence effect. A few figures are presented here to highlight some general aerodynamic features of the BWB model considered in this paper targeting a validation in using the BLI-design tool. Figure 5 illustrates the surface distribution of pressure coefficient, C_p, and skin friction coefficient, C_f, at AoA = 3 and 35, respectively. It is clear that at relatively low AoAs, the boundary layer flow is overall attached, while with increasing AoAs, flow separation starts take place over the upper part of the nose and approaching the leading edge of the wing-body junction area, as indicated by the lower pressures shown in Figure 5(c) and 5(d).

The aerodynamic flow features is further highlighted in Figure 6, where the surface flow pattern is presented to visualize the flow separation over the fore-body part of the fuselage. The flow at the rear part, where the installation of BLI may be located, is attached and cross flows present. At large AoAs, this will certainly modify the availability of the BLI model. To provide an overall view of some general aerodynamic features of the BWB model, Figure 7 shows further the lift, pitching moment, drag polar and L/D, respectively, versus AoAs.

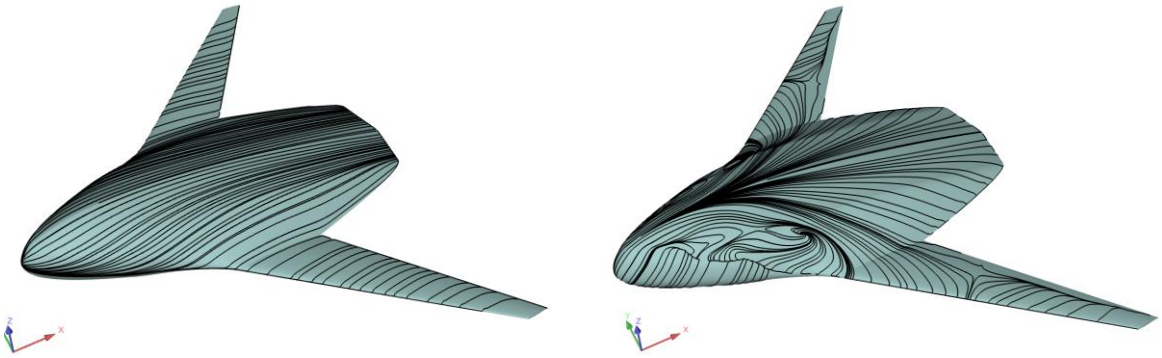

(a) AoA = 3 deg. (b) AoA = 35 Deg.

Figure 6: Examples of CFD simulations. Surface flow patterns at AoA = 3 and AOA = 35 deg.

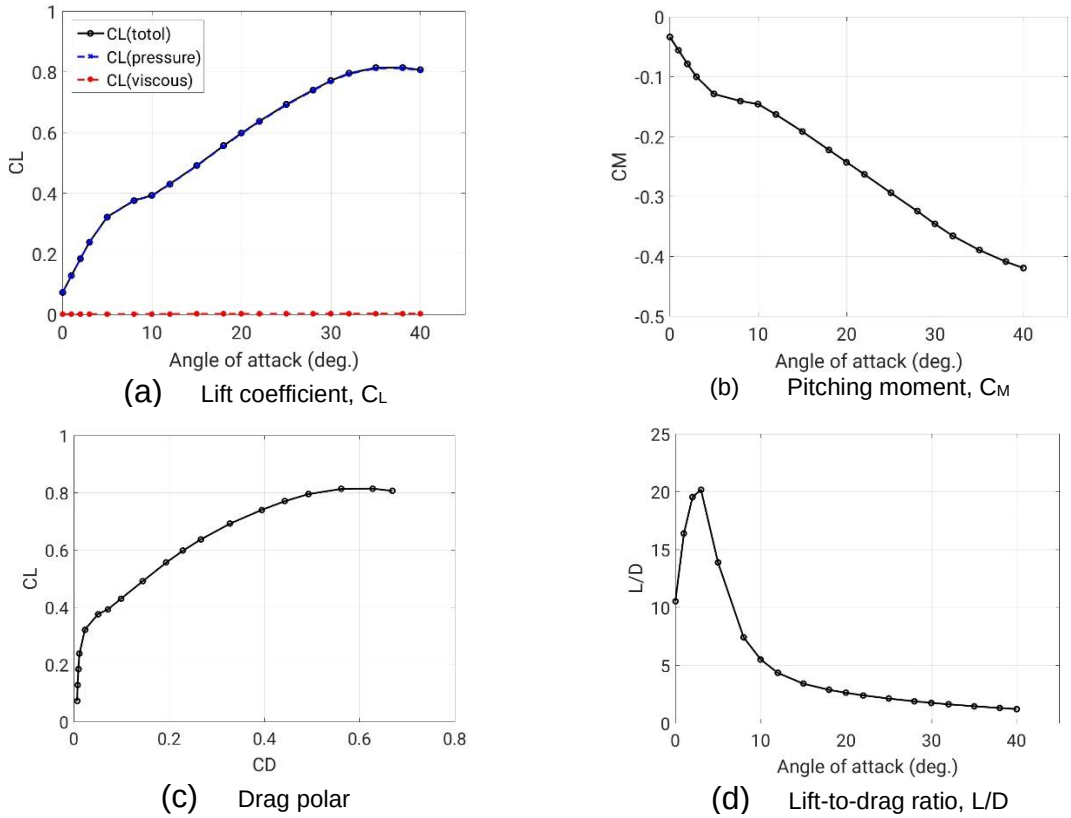

(a) Lift coefficient, C_L (b) Pitching moment, C_M

(c) Drag polar (d) Lift-to-drag ratio, L/D

Figure 7: Aerodynamic forces of the BWB model from CFD simulations for AoA $\in [0,35]$.

4. Validation of the boundary layer estimation method

Within the scope of this paper, the validation of the BLI model focuses on the boundary layer profile calculated using XFOIL and the approximations for typical operations of level flight. Results from the CFD simulations of the baseline BWB, as described in the previous section, are used for the validation. The results of two cases, AoA = 0 deg and AoA = 3 deg, are verified, respectively. For each of the AoA case, the boundary layer velocity profiles at three engine installation positions are extracted and plotted in Figure 8, Figure 9 and Figure 10, respectively.

In general, the comparisons indicate that the boundary layer velocity profile obtained from the present methods are reasonably comparable to the CFD simulation results, under both AoA conditions. At AoA = 0 deg or AoA = 3 deg, both the CFD result and the BLI model prediction give a similar rate of increase in boundary layer thickness. One noticeable observation is, between different positions of the engine installation, the velocity profiles at the outer region of the boundary layer present significant differences in CFD simulations. This behavior is expected as the flow accelerates over the upper side of the airfoil and triggering changes in the boundary layer when the flow moves towards the trailing edge in relation to the circulation effect. The BLI model gives constant value at different installation positions since the freestream velocity is always applied.

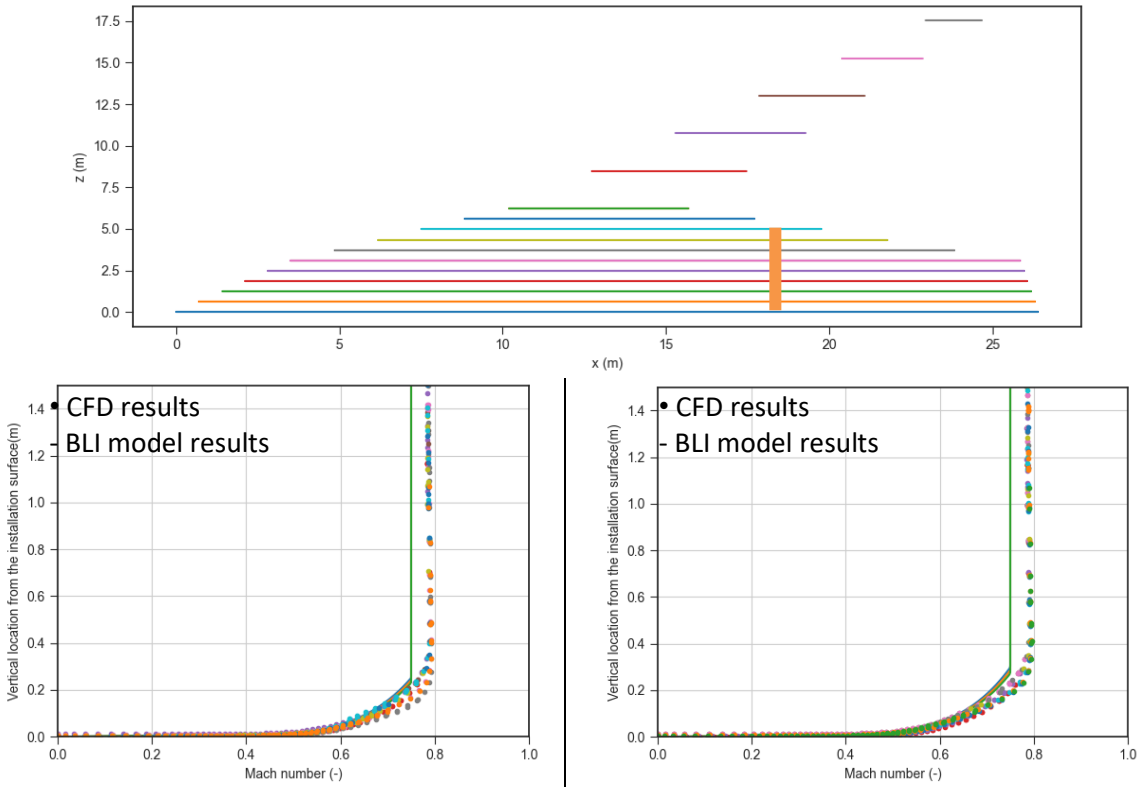

Figure 8: Validation against CFD, 70% fuselage length engine installation position visualization (Top), boundary layer velocity profile @AoA = 0 deg (Bottom left), boundary layer velocity profile @AoA = 3 deg (Bottom right)

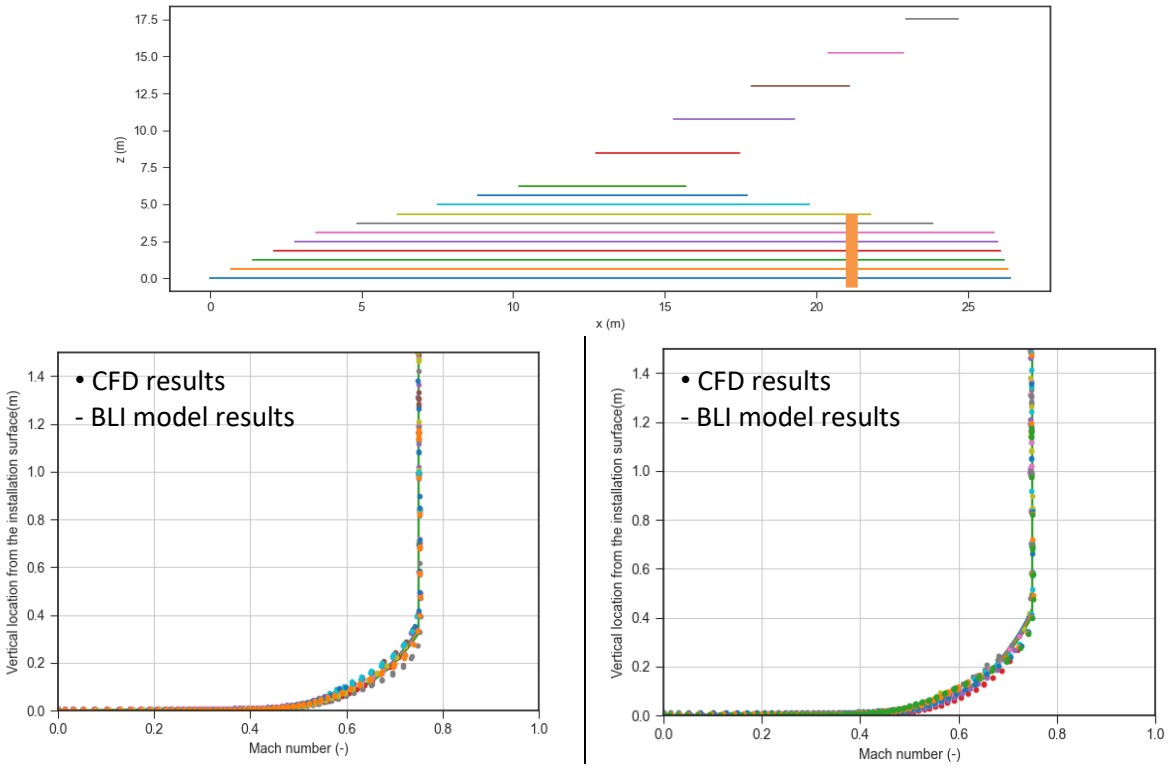

Figure 9: Validation against CFD, 80% fuselage length engine installation position visualization (Top), boundary layer velocity profile @AoA = 0 deg (Bottom left), boundary layer velocity profile @AoA = 3 deg (Bottom right)

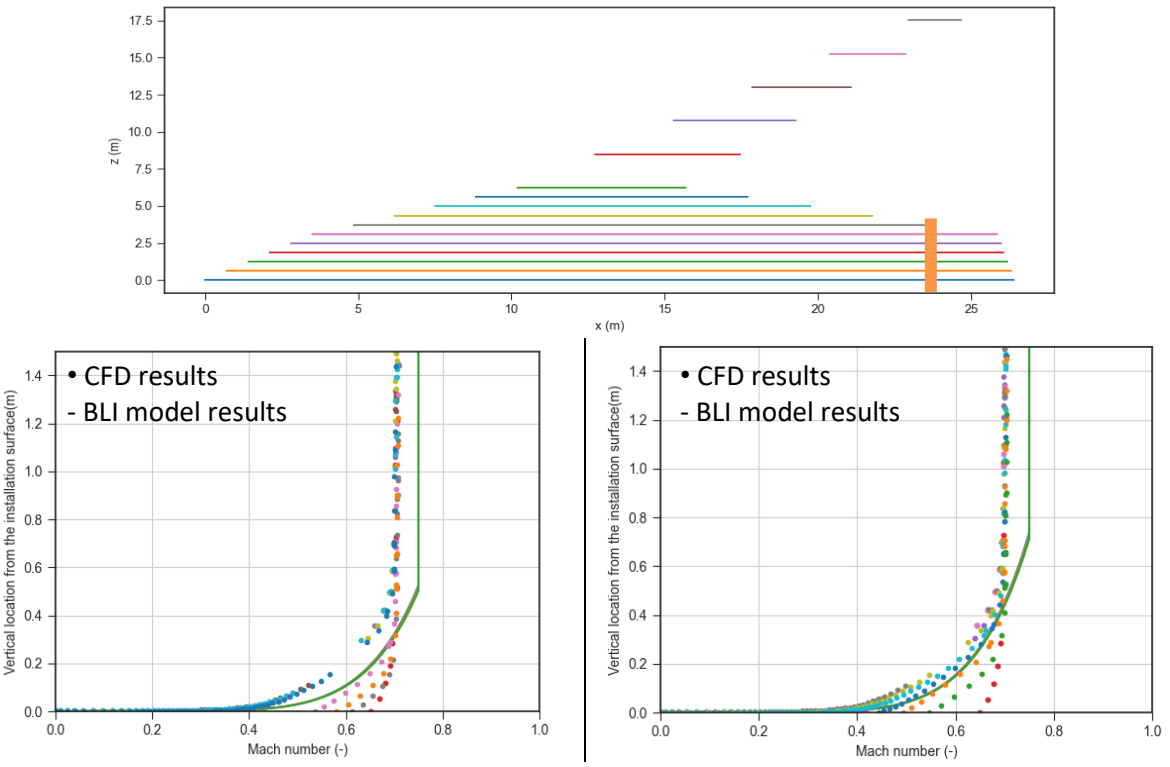

Figure 10: Validation against CFD, 90% fuselage length engine installation position visualization (Top), boundary layer velocity profile @AoA = 0 deg (Bottom left), boundary layer velocity profile @AoA = 3 deg (Bottom right)

Among the three installation positions, the BLI model provides the best prediction when the velocity at the outer region is close to the free-stream velocity. One should always avoid putting the propulsors too close to the trailing edge where the trailing edge effect would deteriorate the fan performance.

Moving the installation upstream, however, may not be beneficial for this BWB as the intake drag increases with the inlet flow velocity. Moreover, the boundary layer growth is insufficient compared to that at downstream positions. However, detailed CFD-based analysis is required to get a more accurate prediction of the outer layer velocity and trailing-edge effect.

5. Summary and PROSPECTS

This paper provides a description of a developed BLI model including related methods incorporated in the aerodynamic analysis tool. The approximations of boundary layer characteristics adopted in the BLI model have been further validated with CFD simulations with an advanced RANS model. By giving the key airframe geometry parameters, flight conditions and BLI fan related parameters as inputs, the proposed BLI model can be used in conceptual designs to estimate the power required and the thrust generated by the fan for a given fan pressure ratio. This includes the fan performance correction considering the inlet flow distortion incurred by the boundary layer ingested.

As a preliminary analysis tool for conceptual design, the model has shown reasonable capabilities of providing the general trend of BLI propulsor performance accounting for the variation of several key design parameters, such as fan inlet corrected mass flow and overall airframe design parameters. The key trade-off between the boundary layer development with different airframe-engine integration and fan preliminary design is reflected. The developed model can be either used standalone or can be easily connected in a framework as a part of the design chain to provide coupled aero-propulsive analysis for BLI configurations.

Acknowledgement

This study is financed by the project IMOTHEP (Investigation and Maturation of Technologies for Hybrid Electric Propulsion)The project has received funding from the European Union's Horizon 2020 research and innovation program under grant agreement number 875006.

References

[1] H. D. Kim, J. L. Felder, M. T. Tong, J. J. Berton, and W. J. Haller, "Turboelectric distributed propulsion benefits on the N3-X vehicle," *Aircraft Engineering and Aerospace Technology: An International Journal,* 2014.

[2] M.-F. Liou, D. Gronstal, H. J. Kim, and M.-S. Liou, "Aerodynamic design of the hybrid wing body with nacelle: N3-X propulsion-airframe configuration," in *34th AIAA Applied Aerodynamics Conference*, 2016, p. 3875.

[3] R. T. Kawai, D. M. Friedman, and L. Serrano, "Blended wing body (BWB) boundary layer ingestion (BLI) inlet configuration and system studies," 2006.

[4] S. Sahoo, X. Zhao, and K. Kyprianidis, "A review of concepts, benefits, and challenges for future electrical propulsion-based aircraft," *Aerospace,* vol. 7, no. 4, p. 44, 2020.

[5] S. Stückl, J. van Toor, and H. Lobentanzer, "VOLTAIR–the all electric propulsion concept platform–a vision for atmospheric friendly flight," in *28th International Congress of the Aeronautical Sciences (ICAS)*, 2012.

[6] H.-J. Steiner, P. C. Vratny, C. Gologan, K. Wieczorek, A. T. Isikveren, and M. Hornung, "Optimum number of engines for transport aircraft employing electrically powered distributed propulsion," *CEAS Aeronautical Journal,* vol. 5, no. 2, pp. 157-170, 2014.

[7] M. Kruger and A. Uranga, "The Feasibility of Electric Propulsion for Commuter Aircraft," in *AIAA SciTech 2020 Forum*, 2020, p. 1499.

[8] D. K. Hall, A. C. Huang, A. Uranga, E. M. Greitzer, M. Drela, and S. Sato, "Boundary layer ingestion propulsion benefit for transport aircraft," *Journal of Propulsion and Power,* vol. 33, no. 5, pp. 1118-1129, 2017.

[9] M. Drela, "Power balance in aerodynamic flows," *AIAA journal,* vol. 47, no. 7, pp. 1761-1771, 2009.

[10] N. Budziszewski and J. Friedrichs, "Modelling of a boundary layer ingesting propulsor," *Energies,* vol. 11, no. 4, p. 708, 2018.

[11] E. S. Hendricks, "A review of boundary layer ingestion modeling approaches for use in conceptual design," *Report, NASA Glenn Research Center,* 2018.

[12] J. Longley and E. Greitzer, "Inlet distortion effects in aircraft propulsion system integration," 1992.

[13] A. Lundbladh and T. Grönstedt, "Distributed propulsion and turbofan scale effects," in *ISABE 2005, 17th Symposium on Airbreathing Engine*, 2005.

[14] A. Rolt and J. Whurr, "Optimizing Propulsive Efficiency in Aircraft with Boundary Layer Ingesting Distributed Propulsion," in *22nd International Symposium on Air Breathing Engines*, 2015, pp. 25-30.

[15] S. Sato, "The power balance method for aerodynamic performance assessment," Massachusetts Institute of Technology, 2012.

[16] A. Uranga *et al.*, "Preliminary experimental assessment of the boundary layer ingestion benefit for the D8 aircraft," in *52nd Aerospace Sciences Meeting*, 2014, p. 0906.

[17] A. Uranga, M. Drela, D. K. Hall, and E. M. Greitzer, "Analysis of the aerodynamic benefit from boundary layer ingestion for transport aircraft," *AIAA journal,* vol. 56, no. 11, pp. 4271-4281, 2018.

[18] A. Rolt and J. Whurr, "Distributed propulsion systems to maximize the benefits of boundary layer ingestion," *ISABE Paper,* vol. 20288, 2015.

[19] M. Brown, "Conceptual Design of Blended Wing Body Airliners Within a Semi-automated Design Framework," 2017.

[20] M. Drela, "An Analysis and Design System for Low Reynolds Number Airfoils. Conf. Paper," in *Conference on Low Reynolds Number Airfoil Aerodynamics, University of Notre Dame, France*, 1989.

[21] N. C. Groves, "An Integral Prediction Method for Three-Dimensional Turbulent Boundary Layers on Rotating Blades," DAVID W TAYLOR NAVAL SHIP RESEARCH AND DEVELOPMENT CENTER BETHESDA MD, 1981.

[22] E. Torenbeek, "Synthesis of subsonic airplane design, 1982," *Delft: Springer*.